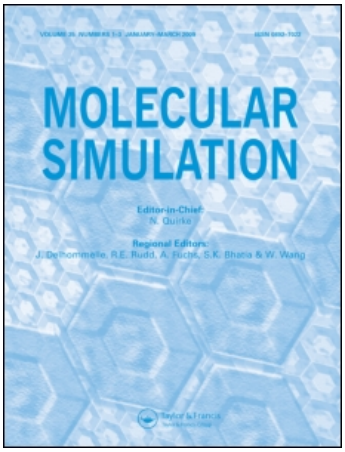

Molecular Simulation
Publication details, including instructions for authors and subscription information:
http://www.informaworld.com/smpp/title~content=t713644482

Water infiltration behaviours in carbon nanotubes under quasi-static and dynamic loading conditions

Guoxin Cao[a]; Yu Qiao[b]; Qulan Zhou[ac]; Xi Chen[a]
[a] Department of Civil Engineering and Engineering Mechanics, Columbia Nanomechanics Research Center, Columbia University, New York, NY, USA [b] Department of Structural Engineering, University of California at San Diego, La Jolla, CA, USA [c] The State Key Laboratory of Power Engineering Multiphase Flow, Xi'an Jiaotong University, Xi'an, P.R. China

To cite this Article Cao, Guoxin , Qiao, Yu , Zhou, Qulan and Chen, Xi(2008) 'Water infiltration behaviours in carbon nanotubes under quasi-static and dynamic loading conditions', Molecular Simulation, 34: 10, 1267 — 1274
To link to this Article: DOI: 10.1080/08927020802175225
URL: http://dx.doi.org/10.1080/08927020802175225

Molecular Simulation
Vol. 34, Nos. 10–15, September–December 2008, 1267–1274

Taylor & Francis
Taylor & Francis Group

Water infiltration behaviours in carbon nanotubes under quasi-static and dynamic loading conditions

Guoxin Cao[a], Yu Qiao[b], Qulan Zhou[ac] and Xi Chen[a]*

[a]*Department of Civil Engineering and Engineering Mechanics, Columbia Nanomechanics Research Center, Columbia University, New York, NY, USA;* [b]*Department of Structural Engineering, University of California at San Diego, La Jolla, CA, USA;* [c]*The State Key Laboratory of Power Engineering Multiphase Flow, Xi'an Jiaotong University, Xi'an, P.R. China*

(*Received 11 January 2008; final version received 1 May 2008*)

The mechanisms of pressure-driven water infiltration into single walled carbon nanotubes are explored using molecular dynamics simulations. Both quasi-static and dynamic loading conditions are investigated, and the influence of tube size is examined. Under quasi-static loading, the water molecules flow into the tube via surface diffusion at a low pressure and when the external pressure reaches a critical value, the infiltrated water flux can sharply increase to a steady state. Upon dynamic loading, the nominal infiltration length per unit external work is employed to measure the comprehensive effect of the loading rate. It is found that such factor is larger (i.e. infiltration is easier) at a lower loading rate and a larger tube size, which is closely related with the interactions between water molecules and nanotube wall atoms.

Keywords: carbon nanotube; water; infiltration; pressure; loading rate

1. Introduction

Due to their excellent combinations of mechanical, electrical and chemical properties, carbon nanotubes (CNTs) have been heavily investigated. Among many subjects, nanofluidic behaviour is a particularly interesting area. Due to the small length scale, large specific surface area and smooth surface, CNTs are excellent candidates for nano-conduits in nanofluidic devices, as well as channels for molecular/ion transport. In fact, controlling nanofluidics is regarded as a key technology for biomedical applications such as molecular sieves, nanopipettes [1], biocatalysis [2] and encapsulation media for storage and transport [3], as well as energy related applications such as energy absorption and damping [4–8].

In order to fulfil these promises, the interaction between nanotube and fluid must be adequately understood. It is of fundamental value to explore the mechanisms of infiltration of water molecules into a single-walled CNT (SWCNT). Conventionally, at the macroscopic scale a surface is referred to as hydrophobic, if it cannot be wetted by water and hydrophilic otherwise. Quantitatively, depending on the contact angle θ, which is the angle between the tangent of the liquid surface with the solid surface at the contact point: if $\theta > 90°$, the surface is hydrophobic; if $\theta < 90°$, it is hydrophilic. The behaviours at nanoscale may be different and whether the inner surface of CNT is hydrophobic or hydrophilic could affect the water infiltration behaviour at the nanoscale.

CNTs might be considered as nonwettable nanopores, since graphite is hydrophobic in continuum experiments [9] and CNTs cannot be dissolved in water; [10] according to which water should not infiltrate into CNTs under ambient condition. However, Dujardin et al. [11] found in their experiments that CNT bundles can be wetted by liquids of surface tensions less than 130–170 mN/m, including water, whose surface tension is 72.8 mN/m at the room temperature. Recently, Rossi et al. [12] used an environmental scanning electron microscopy to study the wetting behaviour of water in CNTs and they found that CNTs produced by chemical vapour deposition with disordered tube walls were hydrophilic, whose contact angles with water were in the range from 5 to 20°. Although, the above experimental results showed that the inner surface of CNTs can be wetted by water, such behaviour is strongly dependent on surface quality. Particularly, impurities and defects may make a hydrophobic surface hydrophilic-like. Therefore, in order to understand the above experimental results, theoretical and numerical studies are necessary.

Molecular dynamics (MD) simulations have been carried out for studying the transport behaviours of molecules inside CNTs [13–17]. For instance, Hummer et al. [18] immersed a very short (6,6) CNT (with the length of about 1.3 nm and with both ends open) in a reservoir with 1000 water molecules, and reported that such an initially empty SWCNT can be filled instantaneously by surrounding water molecules under ambient conditions. We note, however, that there

*Corresponding author. Email: xichen@civil.columbia.edu

ISSN 0892-7022 print/ISSN 1029-0435 online

DOI: 10.1080/08927020802175225
http://www.informaworld.com

may be a few factors affecting the observed spontaneous infiltration behaviour: (1) since the length of the short tube is comparable with the cut-off distance in MD, the water molecules entered the tube from two different ends may interact with each other; (2) the (6,6) tube may be too small and may cause an exceedingly strong interaction between carbon atoms and water molecules; (3) the reservoir (bulk) water molecules outside the tube may interact with the infiltrated molecules, making it difficult to explore the intrinsic property of the inner surface of CNT. During the infiltration of water into CNT bundles or multi-walled CNTs, which accounts for most of the practical applications, the wettability of the inner surface is essential.

Based on MD simulations, Werder et al. [19] reported the effective contact angles of water droplets inside a SWCNT, which was 104.8–136.4°, when the tube diameter varies between 0.82 and 1.63 nm. We caution that such result may not directly imply, whether the water molecules could wet CNTs, since the contact angle is a continuum parameter defined at the macroscopic scale and the results derived from a small cluster of water molecules confined in CNT may not be conclusive, since it is difficult to measure such angles accurately. Significant scatter of data of contact angle computed from MD simulations may overshadow the intrinsic nanofluidic behaviours. A perhaps more reliable measure of wettability (or 'hydrophobicity') at the nanoscale should be based on the details of infiltration behaviour of water in CNTs (including infiltration pressure, infiltration volume and transport of water molecules inside the nanotube), as will be discussed shortly.

At present, most computational works focus on the spontaneous transport behaviours of water molecules inside CNTs under ambient conditions. The study of the pressure-driven infiltration behaviour, i.e. the quasi-static or dynamic entrance of water molecules into a CNT from an outside reservoir upon applied external pressure, is still lacking. We note that during applications such as molecular sieves, nanopipettes, and energy absorption and damping, forces are always applied on the liquids to force them going through the nanopores. The lack of understanding in this area has led to tremendous challenges in developing new nanotube-based nanodevices, including the advanced energy absorption systems and volume-memory liquids [4–8,20,21]. In this paper, MD simulations are employed to explore the mechanisms of water infiltration into a SWCNT under both quasi-static and dynamics loading conditions. Under the quasi-static condition, the effects of pressure and tube size on the infiltration characteristics are investigated; under dynamic loading, the effect of loading rate is explored.

2. Model and computation method

2.1 Computation method

The computational cell includes a rigid SWCNT segment with the length of about 5 nm, and two parallel rigid carbon atom planes which bound a 'reservoir' with the size of 4.65 × 4.65 × 4.65 nm; 3376 water molecules are included inside the reservoir, so as to maintain the normal density of water at ambient condition. (Figure 1). Periodic boundary conditions are applied in the x and y directions of the computational cell. This setting allows water to infiltrate CNT from only one end of the tube and no water molecule may contact the outer surface of the nanopore, thus relieving the constraints [18] mentioned earlier. In order to study the size effect of nanopore, we select three different CNT segments, (20,20), (15,15) and (10,10), with diameters 2.7, 2 and 1.35 nm, respectively. With larger radii than the (6,6) tube used in [18], the interactions between CNT and water molecules will be weaker and thus the more representative infiltration behaviour of CNTs may be obtained.

The MD simulations are carried out by using COMPASS force field [22] in Materials Studio®, in which the intermolecular potential energy of water molecule is described by both the short range Lennard-Jones potential and the Ewald summation of the long range Coulombic potential. A fixed time increment of 1 fs is used. Initially, a rigid cap is imposed on the right end of the empty CNT, and the water molecules in the reservoir are equilibrated for about 50 ps with the NVT ensemble (300 K), during which the Berendsen thermostat is used to keep the temperature constant; the cover is then removed and the infiltration behaviours are monitored for different loading cases described below. The initial structure at 300 K is shown in Figure 1 with initial water density $\rho_0 = 1$ g/cm^3 and initial pressure $P_0 = 10^5$ Pa. Quasi-static or dynamic loads are applied next such that water may enter CNT from its right end.

For the quasi-static cases, the NVT ensemble with the Berendsen thermostat is used to simulate the quasi-static infiltration behaviour of water molecules under different pressure. The pressure of the reservoir, P, can be varied by changing the water density inside the reservoir according to the state equation of water. This is realised by adjusting the right boundary of the reservoir (similar to moving a 'piston'), while pinning the left boundary of the reservoir. At a given pressure level, the position of the piston is fixed

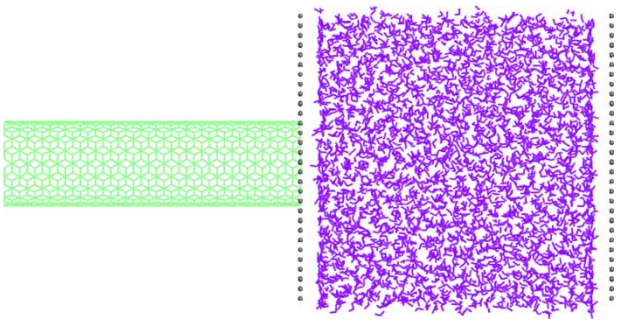

Figure 1. The initial structure before water infiltration into CNT.

during the entire step, and the water infiltration statistics are computed for the next 30 ps.

For the dynamic loading cases, the NVE ensemble is employed to investigate the dynamic infiltration behaviour of water molecules with different loading rates. Four different loading rates of piston are selected in the present work: 1, 0.4, 0.2 and 0.1 nm/ps, and during the simulation the piston moves continuously with such a constant speed. For all loading rates, the final piston displacement is the same, 2 nm.

2.2 *Calculation of pressure in reservoir*

With the movement of piston the reservoir volume is changed, which leads to pressure variation and according to the state equation [23], the water density ρ and pressure P are related as:

$$P = P_0 + 298\left[\left(\frac{\rho}{\rho_0}\right)^{7.15} - 1\right], \tag{1}$$

which is shown in Figure 2. However, Equation (1) may not be suitable to describe the pressure–density relationship of water molecules inside the present computational cell since it is an empirical function fitted from the experimental data of bulk water.

In order to better evaluate the pressure inside the reservoir, we use MD simulations to recalibrate the pressure–density relationship. A new computational cell is established, which has the similar size as the reservoir used above and the initial density of water molecules inside the cell is set as the normal water density, 1 g/cm^3. The periodic boundary conditions are applied in all three directions, so as to simulate the bulk water. The density of water molecules can be varied by reducing the volume of computational cell. For each case, the system is first equilibrated for 20 ps at 300 K by using NVT ensemble, and then the MD simulation (NVE) is run for another 10 ps to calculate the pressure inside the computational cell using:

$$P_{\mathrm{MD}} = \frac{1}{3V}\left(\sum_{i=1}^{N}\sum_{j=1}^{3}\left(m_i v_{i,j}^2 + r_{i,j} f_{i,j}\right)\right), \tag{2}$$

where V is the volume of the computational cell, N is the number of atoms inside the cell, m_i is the mass of atom i, and $v_{i,j}$, $r_{i,j}$, $f_{i,j}$ are the j components of the velocity, position and force vectors of the ith atom, respectively ($j = 1$–3). The calculated pressure values are averaged for 10 ps and fitted in a form that is similar to Equation (1) (Figure 2):

$$P = P_0 + 513\left[\left(\frac{\rho}{\rho_0}\right)^{4.8} - 1\right]. \tag{3}$$

Figure 2 shows that when the pressure is lower than about 600 MPa (or when the water density variation is smaller than about 16%), there is a good agreement between the MD simulation and the state Equation (1); however, Equation (1) significantly overestimates the pressure when the density variation is larger. Note that state Equation (1) was fitted from experiments upon moderately small water density variation [23] and its application to high pressure may be problematic. In this paper, we use Equation (3), which is validated at lower pressures, to calculate the pressure of water molecules in reservoir in a wider range.

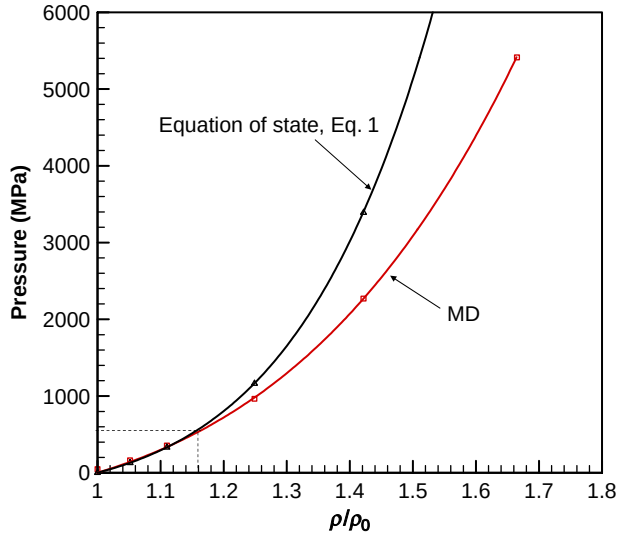

Figure 2. The relationship between water density variation and reservoir pressure.

3. Conformation of water molecules inside nanotubes

The conformation of water molecules inside CNTs may be different when loading rate and/or tube size changes. The radial density profile (RDP) is a convenient way to illustrate the conformation of the infiltrated water molecules inside the tube, as the tube radius and loading rate are varied. The RDP is defined as $g_r = n_r/(2\pi r \Delta r n_{\mathrm{in}})$, where n_{in} is the total number of infiltrated water molecules and n_r is the number of subset water molecules distributed within an annular space with inner radius r and outer radius $r + \Delta r$, with respect to the tube axis.

Figure 3(a) and (b) show the RDP of infiltrated water molecules under quasi-static and dynamic conditions with different loading rates, for (10,10) and (20,20) tubes, respectively; the data are averaged when the piston displacement varies from 1.8 to 2 nm. The results show that at the highest loading rate, 1 nm/ps, the RDP is more uniform and the formation of the first solvation shell is not

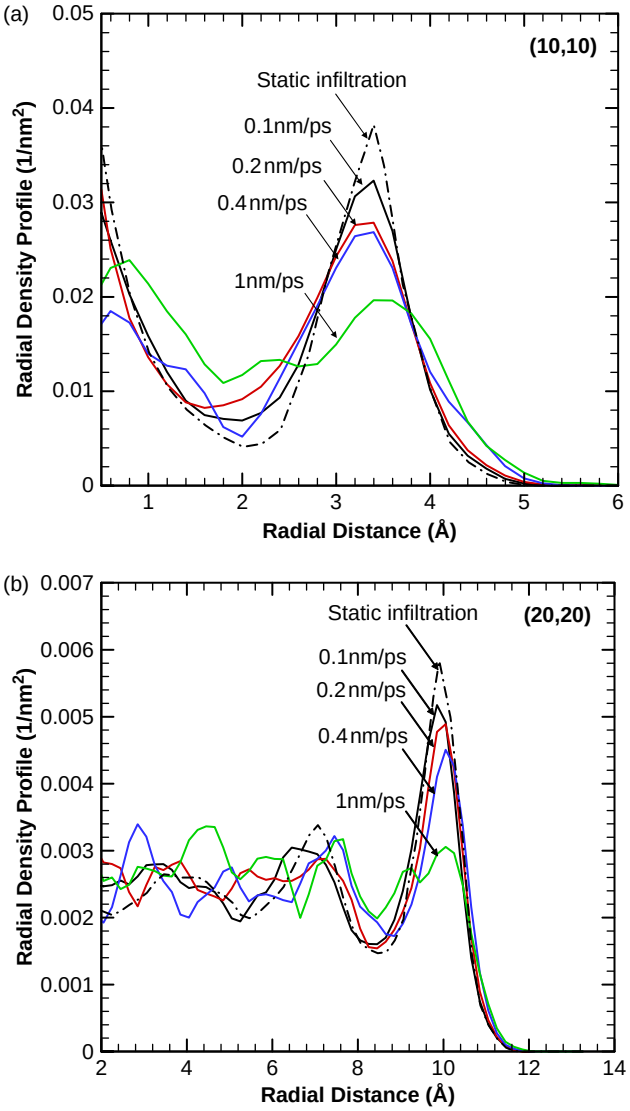

Figure 3. The RDPs for water molecules inside nanotubes, (a) (10,10); (b) (20,20) tube.

obvious. With the decrease of the loading rate, the first solvation shell becomes more prominent, and the RDP converges to that under quasi-static condition, which has the highest magnitude of the first solvation shell. To quantify the conformational difference at different loading rates, we introduce an effective distributed radius of the infiltrated water molecules, $\bar{R}$, which is the radius of the cylindrical space containing 95% of the infiltrated water volume. According to Table 1, $\bar{R}$ is the lowest for quasi-static infiltration and it increases with the increase of the loading rate. For (20,20), (15,15) and (10,10) tubes, within the range of loading rates studied in this paper, their effective distributed radius increase by 0.136, 0.349 and 0.385 Å, respectively. This should be attributed to that in a smaller tube the carbon atoms have a more prominent interaction with water molecules.

Under the quasi-static condition, water infiltration is dominated by the surface diffusion (see the next section) and the driving force is the free energy difference between the water molecules inside and outside the tube. The conformation of water molecules inside the tube is strongly affected by its non-bonded interaction with the tube wall, which leads to the formation of the first solvation shell (at the equilibrium distance of about 3.3 Å from the tube wall), so as to reduce the system free energy. With increasing loading rate, the entry water molecules have higher velocities that are governed by the direct kinetic energy transfer from the piston to water molecules. Upon dynamic loading, there is no sufficient time for the infiltrated water molecules to adjust their positions toward the equilibrium positions according to the van der Waals interaction with tube wall, and they have to move primarily along the axial direction. Therefore, the formation of the first solvation shell is not obvious and the effective distributed radius is larger at higher loading rates.

4. Quasi-static infiltration behaviour

We first explore the infiltration mechanisms upon quasi-static loading. In order to decouple the size effect, we define a nominal quasi-static infiltration length, $\tilde{L}$, which is the ratio of the infiltrated water volume to the effective distributed area of H_2O molecules in the tube, $\tilde{L} = V_{in}/\pi\bar{R}^2$. The relationship between reservoir pressure and nominal infiltration length is shown in Figure 4. It is interesting that under an ambient pressure of 1 atm (0.1 MPa), a number of water molecules may 'spontaneously' enter the tube. In order to infiltrate into the tube, the reservoir (bulk) water molecules must overcome an energy barrier to lose at least two hydrogen bonds [18], which requires the relative higher activation energy than that provided by the random thermal vibration. However,

Table 1. The effective distributed radius of infiltrated water molecules under different loading rates.

		Effective distributed radius under different loading rates (Å)			
Nanotube	Tube radius (Å)	0.1 nm/ps	0.2 nm/ps	0.4 nm/ps	1 nm/ps
(10,10)	6.708	4.247	4.338	4.515	4.632
(15,15)	10.033	7.33	7.432	7.511	7.679
(20,20)	13.361	10.556	10.625	10.687	10.713

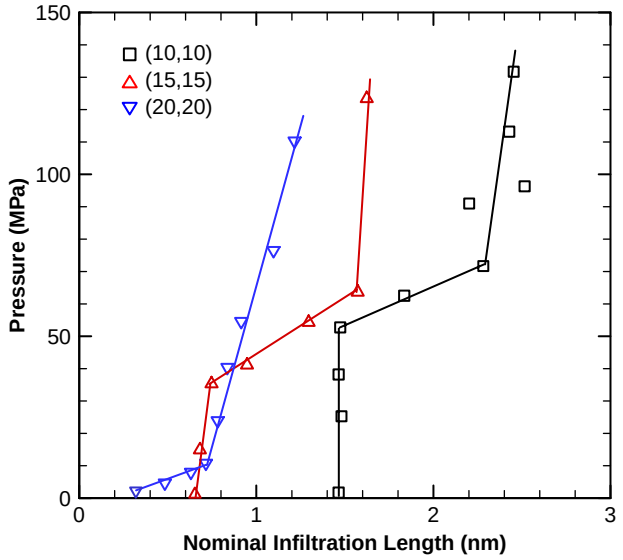

Figure 4. The relationship between the nominal infiltration length $\tilde{L}$ and reservoir pressure P.

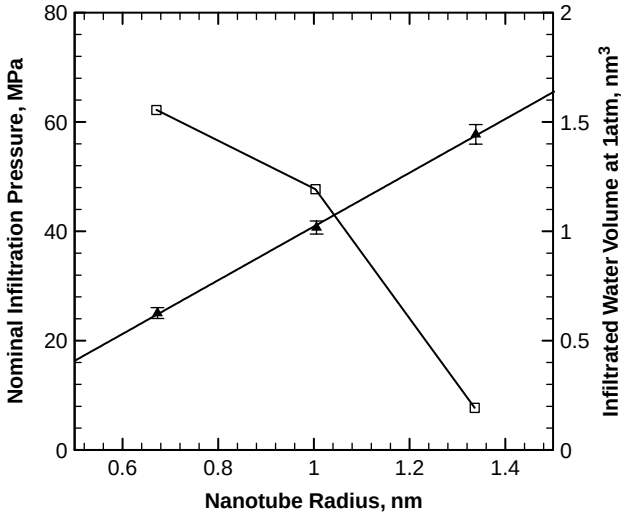

Figure 5. The relationship between the nominal infiltration pressure and nanotube radius (square symbol), and the relationship between the nanotube size and infiltrated water volume at 1 atm (triangular symbol).

due to the help of the van der Waals attraction of the tube, the energy barrier of water molecules near to the tube opening is significantly reduced, and thus the water molecules near tube opening may enter the tube via surface diffusion (with the help of thermal vibration).

With the increase of the reservoir pressure, P, Figure 4 shows that the relationship between the nominal infiltration length and the pressure is highly nonlinear. Without losing generality, based on the P–$\tilde{L}$ relationship, the infiltration process can be divided into three stages: (1) $\tilde{L}$ increases very slowly with P at low pressure values; (2) when the pressure gets beyond a certain value, $\tilde{L}$ increases quickly; (3) afterwards, the water fluence increases slowly with the continued increase of P. As an external pressure is applied, the free energies of bulk water molecules rise accordingly. When the pressure is relatively low, most reservoir water molecules cannot directly overcome the energy barrier, and only those near the tube edge may rely on the surface diffusion mechanism to enter the CNT; this is the first stage in Figure 4. When the pressure reaches a critical value, P_{in}, also termed as the nominal infiltration pressure, the energy barrier can be overcome by most of bulk water molecules, leading to a sharp increase in the nominal infiltration length, which is the second stage in Figure 4. Further, increase of the external pressure has no pronounced effect on the infiltration, since there are no other primary energy barriers. This phenomenon is different from the phenomena at the macro-scale. For a hydrophilic surface, the capillary pressure will spontaneously drive the liquid into the tube without the requirement of an additional external pressure; for a hydrophobic surface, the liquid should first overcome the capillary effect. In the case of CNTs under investigation, it shows a mixed characteristic of both.

The nominal infiltration pressure is size-dependent. Figure 5 shows the relationship between P_{in} and nanotube radius. With the increase of tube size, the decrease of P_{in} becomes more and more prominent. For a tube with larger radius (and also smaller surface area per volume), the free energy difference between water molecules inside and outside CNT is smaller, which leads to a reduced infiltration energy barrier. Therefore, a smaller perturbation is required for water infiltration, resulting in a lower nominal infiltration pressure.

5. Effect of loading rate on dynamic infiltration behaviour

Under the dynamic loading, the infiltration behaviour is more complicated than its quasi-static counterpart. Several factors are coupled, including loading rate, reservoir pressure and overall infiltration time. A new variable is needed to show the comprehensive effect. The piston does work to the system continuously, which can be expressed as:

$$W = \int P(t)\mathrm{d}V = \int P(t)S\,\mathrm{d}l, \tag{4}$$

where $P(t)$ is the reservoir pressure calculated by Equation (3), which is a function of time; $\mathrm{d}V$ is the volume decrement of the reservoir; S is the cross-section area of the piston; and $\mathrm{d}l$ is the displacement increment of the piston. The effective dynamic infiltration length is defined as $\tilde{L}_{\text{d}} = V_{\text{in}}/\pi\bar{R}^2W$, which reflects the infiltration length per unit work done by piston and a larger $\tilde{L}_{\text{d}}$ means that the water infiltration is easier.

Figure 6(a)–(c) shows the relationship between the normalised infiltrated water volume, $V_{\text{in}}/V_{\text{in}}^{\max}$, and $\tilde{L}_{\text{d}}$

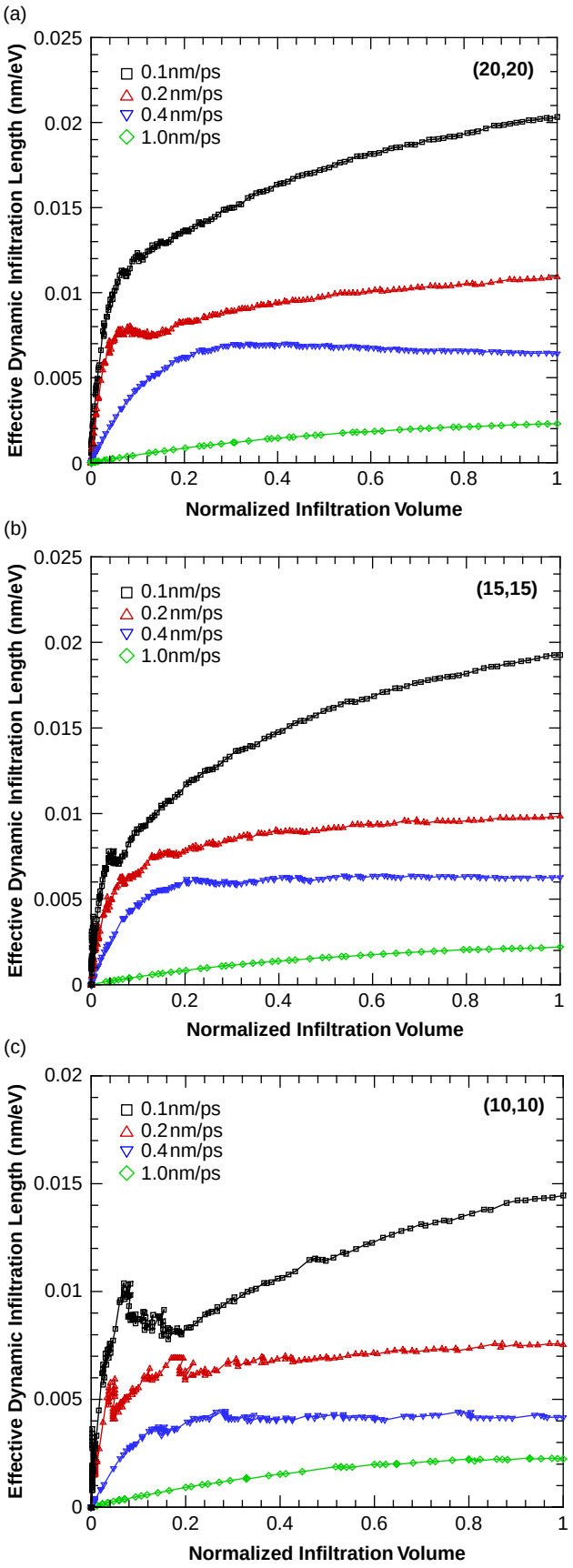

Figure 6. The effective dynamic infiltration length as a function of the normalised infiltration volume, (a) (20,20); (b) (15,15) and (c) (10,10) tube.

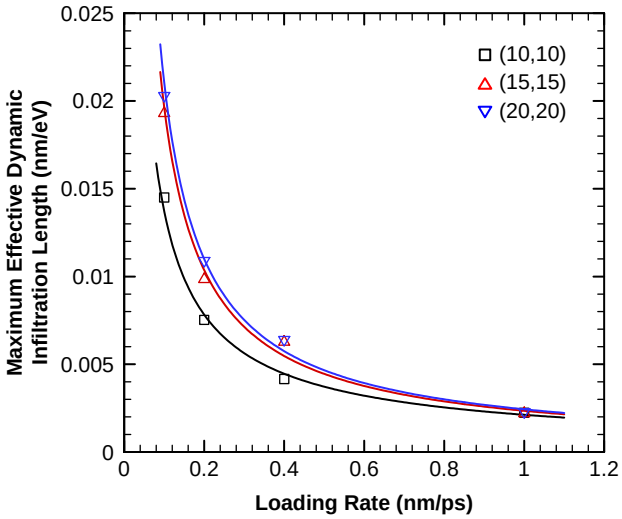

Figure 7. The relationship between the $\tilde{L}_{\mathrm{d}}^{\max}$ and the loading rate for different tube sizes.

under different loading rates. For the slowest loading rate (0.1 nm/ps), $\tilde{L}_{\mathrm{d}}$ first quickly increases when V_{in} is small and then the increasing rate is much reduced when $V_{\mathrm{in}} > 0.1\,V_{\mathrm{in}}^{\max}$; for the loading rate of 0.2 nm/ps, the trend is similar, but $\tilde{L}_{\mathrm{d}}$ increases much slower with V_{in}, when $V_{\mathrm{in}} > 0.1V_{\mathrm{in}}^{\max}$; for the loading rate of 0.4 nm/ps, the initial increasing slope of $\tilde{L}_{\mathrm{d}}$ is significantly reduced and after $V_{\mathrm{in}} > 0.2V_{\mathrm{in}}^{\max}$, $\tilde{L}_{\mathrm{d}}$ becomes essentially insensitive to V_{in}; when the loading rate is 1 nm/ps, $\tilde{L}_{\mathrm{d}}$ increases slowly with V_{in} during the entire infiltration process. Denote $\tilde{L}_{\mathrm{d}}^{\max}$ as the value of $\tilde{L}_{\mathrm{d}}$ at the maximum infiltration volume, $V_{\mathrm{in}}^{\max}$.

The infiltration procedure can be divided into two stages: (1) the water molecules infiltrate into the nanotube from the reservoir; (2) the infiltrated water molecules then transport inside the nanotube. The first stage needs a much lower work than the second stage because in the second stage, there is a periodic energy barrier arisen from the nanotube lattice, similar to 'friction force' and thus $\tilde{L}_{\mathrm{d}}$ is significantly increased with the increase of the normalised infiltration volume in the initial stage, and then such increasing trend in the second stage is sharply reduced due to the lattice resistance. The resistance increases with the increase of infiltration volume, since it linearly scales with the contact area between the infiltrated water molecules and the tube wall. In addition, a higher loading rate will cause a higher resistance and thus it needs more work for water molecules to transport inside tube, which can be further verified in Figure 8. Therefore, the slope of the second stage in Figure 6 decreases with the increase of the loading rate,

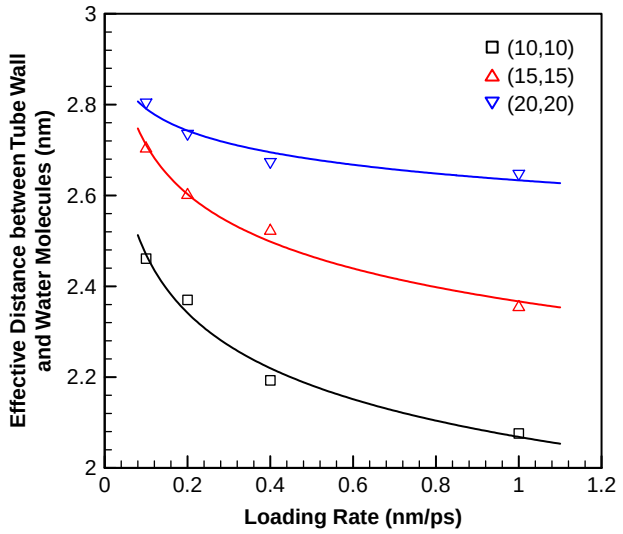

Figure 8. The relationship between the effective water molecules-nanotube wall distance ($R - \bar{R}$) and the loading rate for different nanotubes.

and it even becomes negative for water molecules inside a (20,20) tube with the loading rate of 0.4 nm/ps. Figure 7 shows that with the increase of loading rate, $\tilde{L}_{\mathrm{d}}^{\max}$ is significantly lowered. In addition, the easiness of infiltration is enhanced for the larger tube.

The effect of loading rate primarily arises from the energy barriers due to nanoscale confinement: when the infiltrated water molecules transport along the axial direction, they must overcome the periodic energy barriers imposed by the carbon atoms. While, such barrier is negligible on quasi-static water transportation, it becomes more prominent at higher loading rates. In essence, the resistance caused by energy barrier is due to the van der Waals interactions between the water molecules and carbon atoms, which increases nonlinearly when their distances become shorter. In the present work, we use the full atomic water model (TIP3P), which includes one oxygen atom and two hydrogen atoms. Since the Van der Waals interaction between the carbon atoms and oxygen atoms is much larger than that between the carbon atoms and hydrogen atoms, the energy barrier of water molecules transporting inside a CNT is mainly from the energy barrier of the transportation of oxygen atoms. Figure 8 shows that the effective distance between the tube wall and water molecules, $R - \bar{R}$, increases with the decrease of loading rate and the increase of tube radius, where R is the tube radius. Such variation trend qualitatively agrees with that of $\tilde{L}_{\mathrm{d}}^{\max}$ in Figure 7, which shows that $R - \bar{R}$, which is closely related with the energy well due to confinement, is coupled with the easiness of infiltration upon dynamic loading. At a higher loading rate, $\bar{R}$ is larger in a smaller tube which leads to relatively closer distances between water molecules and carbon atoms, and thus a higher resistance force is generated, which makes infiltration more difficult, in terms of more work needed for the same nominal infiltration length. This argument can also be supported by Figure 3(a) and (b). The results suggest that the energy absorption density of hydrophobic nanoporous materials can be enhanced upon dynamic loading, which agrees with experiment data [5].

6. Conclusion

By using MD simulations, we study the mechanisms of pressure-driven water infiltration into a SWCNT under both quasi-static and dynamic loading conditions, with the factor of tube size being taken into consideration. Under quasi-static condition, the infiltration process is driven by the free energy difference between water molecules inside and outside the tube and it primarily relies on surface diffusion at lower pressure. When the applied pressure is not yet significant, only those molecules close to the tube entrance having higher energies can overcome the energy well and enter the tube, with the assistance of thermal fluctuation and van der Waals attraction. With the increase of external pressure the entrance of water molecules becomes easier and at a critical pressure all prominent barriers can be overcome and the nominal infiltration length sharply increases, which eventually approaches to a steady state. The nominal infiltration pressure decreases with the increase of tube diameter.

Upon dynamic loading, the main driving force of infiltration is the external work, which can be directly transferred to the kinetic energy of water molecules. The nominal infiltration length per unit external work, $\tilde{L}_{\mathrm{d}}$, is introduced to show the comprehensive effect of the loading rate. It is found that $\tilde{L}_{\mathrm{d}}$ is larger at a lower loading rate and a larger tube size; such phenomenon is closely connected to the interaction between water molecules and nanotube wall, which imposes a resistance to water transport. With a lower loading rate and/or larger tube size, the effective distributed radius of infiltrated water molecules is smaller, which suggests that the averaged distance between carbon atoms and water molecules is larger, causing a weaker interaction and making the infiltration easier.

The main findings of present work can be extended to other nano-environments such as CNT bundles, multi-walled CNTs, or microporous materials, e.g. zeolites and zeolite-like materials. One of the future works can be extended to explore the behaviours of water solutions with different solutes and the effect of ions [24–27]. Such study will be very useful for the potential of employing the nanoporous materials and nanotubes for energy absorption and damping [4–8], which relies on the excessive interface energy between the liquid and nanoporous solid. When solutes are placed in water, the infiltration energy landscape is changed and that provides a versatile platform for tailoring the energy absorption and damping capabilities.

Such studies will be reported in the future and it is suspected that the effect of ions will be coupled with the loading rate effect [24], and thus the effect of ions may be more clearly revealed after the intrinsic loading rate effect and infiltration behaviour of pure water are understood in this study.

Acknowledgements

The study was supported by The Army Research Office under Grant no. W911NF-05-1-0288 and by National Science Foundation CMMI-0643726.

References

[1] M.-H. Hong, K.H. Kim, J. Bae, and W. Jhe, *Scanning nanolithography using a material-filled nanopipette*, Appl. Phys. Lett. 77 (2000), pp. 2604–2606.
[2] D.T. Mitchell, S.B. Lee, L. Trofin, N. Li, T.K. Nevanen, H. Söderlund, and C.R. Martin, *Smart nanotubes for bioseparations and biocatalysis*, J. Am. Chem. Soc. 124 (2002), pp. 11864–11865.
[3] A. Kalra, S. Garde, and G. Hummer, *Osmotic water transport through carbon nanotube membranes*, Proc. Natl Acad. Sci. USA 100 (2003), pp. 10175–10180.
[4] A. Han and Y. Qiao, *Infiltration pressure of a nanoporous liquid spring modified by an electrolyte*, J. Mater. Res. 22 (2007), pp. 644–648.
[5] F.B. Surani, X. Kong, and Y. Qiao, *Energy absorption of a nanoporous system subjected to dynamic loadings*, Appl. Phys. Lett. 87 (2005), 163111.
[6] V.K. Punyamurtula and Y. Qiao, *Hysteresis of sorption isotherm of a multiwall carbon nanotube in paraxylene*, Mater. Res. Innov. 11 (2007), pp. 37–39.
[7] A. Han and Y. Qiao, *A volume memory liquid*, Appl. Phys. Lett. 91 (2007), 173123.
[8] X. Chen, F.B. Surani, X. Kong, V.K. Punyamurtula, and Y. Qiao, *Energy absorption performance of a steel tube enhanced by a nanoporous material functionalized liquid*, Appl. Phys. Lett. 89 (2006), 241918.
[9] A.W. Adamson and A.P. Gast, *Physical Chemistry of Surfaces*, 6th ed., John Wiley & Sons, New York, 1997.
[10] J. Liu, A.G. Rinzler, H. Dai, J.H. Hafner, R.K. Bradley, P.J. Boul, A. Lu, T. Iverson, K. Shelimov, C.B. Huffman et al., *Fullerene pipes*, Science 280 (1998), pp. 1253–1256.
[11] E. Dujardin, T.W. Ebbesen, A. Krishnan, and M.M.J. Treacy, *Wetting of single shell carbon nanotubes*, Adv. Mater. 10 (1998), pp. 1472–1475.
[12] M.P. Rossi, H. Ye, Y. Gogotsi, S. Babu, P. Ndungu, and J.-C. Bradley, *Environmental scanning electron microscopy study of water in carbon nanopipes*, Nano Lett. 4 (2004), pp. 989–993.
[13] A. Striolo, *The mechanism of water diffusion in narrow carbon nanotubes*, Nano Lett. 6 (2006), pp. 633–639.
[14] K. Koga, G.T. Gao, H. Tanaka, and X.C. Zeng, *Formation of ordered ice nanotubes inside carbon nanotubes*, Nature 412 (2001), pp. 802–805.
[15] Y. Liu, Q. Wang, T. Wu, and L. Zhang, *Fluid structure and transport properties of water inside carbon nanotubes*, J. Chem. Phys. 123 (2005), 234701.
[16] J. Martí and M.C. Gordillo, *Temperature effects on the static and dynamic properties of liquid water inside nanotubes*, Phys. Rev. E 64 (2001), 021504.
[17] B. Huang, Y. Xia, M. Zhao, F. Li, X. Liu, Y. Ji, and C. Song, *Distribution patterns and controllable transport of water inside and outside charged single-walled carbon nanotubes*, J. Chem. Phys. 122 (2005), 084708.
[18] G. Hummer, J.C. Rasaiah, and J.P. Noworyta, *Water conduction through the hydrophobic channel of a carbon nanotube*, Nature 414 (2001), pp. 188–190.
[19] T. Werder, J.H. Walther, R.L. Jaffe, T. Halicioglu, F. Noca, and P. Koumoutsakos, *Molecular dynamics simulation of contact angles of water droplets in carbon nanotubes*, Nano Lett. 1 (2001), pp. 697–702.
[20] Y. Qiao, V.K. Punyamurtula, A.J. Han, X.G. Kong, and F.B. Surani, *Temperature dependence of working pressure of a nanoporous liquid spring*, Appl. Phys. Lett. 89 (2006), 251905.
[21] Y. Qiao, G.X. Cao, and X. Chen, *Effects of gas molecules on nanofluidic behaviors*, J. Am. Chem. Soc. 129 (2007), pp. 2355–2359.
[22] H. Sun, *COMPASS: An* ab initio *force field optimized for condensed-phase applications, overview with details on alkane and benzene compounds*, J. Phys. Chem. B 102 (1998), pp. 7338–7364.
[23] P.G. Tait, *Report on some of the physical properties of fresh water and sea water*, Phys. Chem. 2 (1888), pp. 1–17.
[24] L. Liu, Y. Qiao, and X. Chen, *Pressure-driven water infiltration into carbon nanotube: the effect of applied charges*, Appl. Phys. Lett. 92 (2008), 101927.
[25] G. Cao, X. Chen, C. Li, A. Ji, and Z. Cao, *Self-assembled triangular and labyrinth buckling patterns of thin films on spherical substrates*, Phys. Rev. Lett. 100 (2008), 036102.
[26] X. Chen and J.W. Hutchinson, *A family of herringbone patterns in thin films*, Script. Mat. 50 (2004), pp. 797–801.
[27] V. Gordon, X. Chen, J.W. Hutchinson, A.R. Bausch, M. Marquez, and D.A. Weitz, *Self-assembled inflated polymer membrane capsules inflated by osmotic pressure*, J. Am. Chem. Soc. 126 (2004), pp. 14117–14122.